Zonal Flow Vacillation and Bimodality of Baroclinic Eddy Life Cycles in a Simple Global Circulation Model

KOJI AKAHORI AND SHIGEO YODEN

Department of Geophysics, Kyoto University, Kyoto, Japan

(Manuscript received 28 June 1996, in final form 8 January 1997)

ABSTRACT

A global primitive-equation model of the atmosphere is used to study the relationship between the temporal variations of the zonal mean zonal flow and baroclinic eddies. Nonperiodic low-frequency vacillation of the mean zonal flow is found in longtime integrations of the model under a perpetual condition; the zonal-mean jet in the extratropics changes its position nearly barotropically.

A potential vorticity–potential temperature (PV–θ) analysis is performed for two extreme periods of the zonal flow vacillation. Anticyclonic breakings of upper troughs are dominant in the period of a high-latitude jet, while cyclonic breakings are dominant in the period of a low-latitude jet. A statistically significant relationship between the zonal flow vacillation and the morphology of life cycles of baroclinic eddies is obtained for the entire period analyzed. An index of the life cycles, which is introduced in this study, shows clear bimodality in its frequency distribution function.

The relationship is also confirmed by two experimental runs with a different intensity of the surface drag. For the low-drag run, the zonal-mean jet is located in high latitudes through the integration period and life cycles of baroclinic eddies are basically characterized by the anticyclonic breaking. For the high-drag run, on the other hand, the zonal-mean jet is located in low latitudes and life cycles of baroclinic eddies are characterized by the cyclonic breaking.

Although these two types of breaking pattern are similar to the two paradigms of baroclinic wave life cycles obtained in some idealized one-shot experiments, there are some differences from the one-shot experiments in the deformation field on an isentropic surface and in the relative location between the zonal-mean jet and the latitude of maximum eddy kinetic energy.

1. Introduction

Low-frequency variations of the zonal mean zonal flow, which are characterized by the irregular emergence of two extreme phases of barotropic zonal flow deviations centered around 40°S and 60°S, have been observed in the Southern Hemisphere winter (e.g., Yoden et al. 1987). Karoly (1990) pointed out that they are caused by interactions between the mean zonal flow and transient eddies; when the mean zonal flow is strong at high latitudes, transient baroclinic eddies are also active in high latitudes and maintain the extreme zonal flow.

Yu and Hartmann (1993) obtained such a zonal flow vacillation in a longtime (3070 days) integration of a simplified general circulation model (GCM) with zonally symmetric forcing under a perpetual equinox condition. They showed evidence of interactions between the mean zonal flow and baroclinic eddies by analysis of eddy fluxes. Similar results were also obtained by James and James (1992) and James et al. (1994) in some 100-yr runs of a simplified GCM under a perpetual solstice condition, although they have little intention of applying their results to the Southern Hemisphere.

In the last two decades, nonlinear behavior of baroclinic waves has been investigated by one-shot experiments as an initial value problem, in which idealized zonally symmetric states are perturbed with small-amplitude disturbances without any zonally symmetric restoring forces. Simmons and Hoskins (1980) obtained strikingly different nonlinear behaviors, denoted as "basic" and "anomalous" life cycles, for two initial states with the same temperature field but a different zonal flow in the horizontal shear. Thorncroft et al. (1993, hereafter THM) examined the two idealized baroclinic wave life cycles from a potential vorticity–potential temperature (PV–θ) perspective (Hoskins et al. 1985). For the initial state of the basic westerly jet, the nonlinear stage of the baroclinic waves developed from a small perturbation of the most unstable mode is characterized by backward-tilted, thinning troughs being advected anticyclonically and equatorward; this life cycle was denoted by LC1 and an "anticyclonic" behavior. For the anomalous case of the initial zonal flow with a superposition of the barotropic component, the life cycle is characterized by forward-tilted, broadening troughs

Corresponding author address: Dr. Shigeo Yoden, Department of Geophysics, Kyoto University, Kyoto 606-01, Japan.
E-mail: yoden@kugi.kyoto-u.ac.jp

wrapping themselves up cyclonically and poleward, producing major cutoff cyclones in high latitudes. This was also denoted by LC2 and a "cyclonic" behavior. Recently, Magnusdottir and Haynes (1996) applied the wave-activity diagnostics to several baroclinic wave life cycles, including LC1 and LC2. Hartmann and Zuercher (1997) also made a numerical study by changing the intensity of barotropic shear and found an abrupt transition from LC1-type to LC2-type behavior in a narrow range of the shear parameter.

These two paradigms of the behavior of midlatitude cyclones have been observed in the real atmosphere. Appenzeller and Davies (1992) and Appenzeller et al. (1996) obtained some typical examples over Europe and found very different behavior for each cyclone. Hartmann (1995) analyzed PV patterns of transient baroclinic eddies in the Southern Hemisphere winter in two extreme periods of the zonal flow vacillation. The anticyclonic behavior of the LC1-type cyclones is observed in almost all longitudes when the zonal mean westerly jet is broad with local maxima near 30°S and 60°S. On the other hand, the cyclonic behavior of the LC2-type cyclones is observed when the zonal-mean jet is narrow with a peak near 40°S. It was suggested that the zonal flow vacillation is caused by a mutual interaction between the barotropic shear of the westerly jet and the behavior of baroclinic eddy life cycles.

In this paper, we elucidate the relationship between the zonal flow vacillation and the two paradigms of baroclinic eddy life cycles by longtime integrations of a high-resolution model that enables us to perform a PV–θ analysis. After we had almost accomplished this work, a numerical study on the two paradigms of baroclinic eddy life cycles with a similar simplified GCM was reported by Lee and Feldstein (1996). However, their motivations and analyses are considerably different from ours; they clarified the wave breakings as a longitudinally localized phenomenon near the center of wave-packet motion but did not investigate the relationship with zonal flow vacillation very much.

Our model is described in section 2. The results of the control run are given in section 3 and those of two experimental runs are in section 4. Discussion is given in section 5 and conclusions are in section 6.

2. Model

Our model is based on the AGCM5 code of the GFD-DENNOU Library. It is a spectral primitive-equation model with triangular truncation at total wavenumber 42 and with 20 σ levels in the vertical. The horizontal resolution is as high as the model used by Simmons and Hoskins (1980), in which evolutions of baroclinic eddies are well described. The σ levels are given in Table 1; the bottom 13 levels are nearly equal to those in THM and the top 6 levels are sponge layers, preventing wave reflections at the top boundary $\sigma = 0$ where $\dot{\sigma} = 0$ is assumed. These spatial resolutions are much higher than those used in the previous longtime integrations by James and James (1992) and Yu and Hartmann (1993).

TABLE 1. Vertical σ levels of the present model and vertical profiles of $T_0(\sigma)$, $\Delta T(\sigma)$, and $\tau_N(\sigma)$.

	Level					
	1	2	3	4	5	6
σ	0.963	0.881	0.782	0.675	0.572	0.480
T_0 (K)	283.1	278.7	272.8	265.6	257.6	249.4
ΔT (K)	59.9	59.6	59.0	57.7	54.6	49.6
τ_N (day^{-1})	15.0	15.0	15.0	15.0	15.0	15.0
	Level					
	7	8	9	10	11	12
σ	0.403	0.340	0.288	0.241	0.196	0.151
T_0 (K)	241.2	233.4	225.9	219.3	214.4	211.3
ΔT (K)	43.3	36.7	30.5	22.4	13.2	4.6
τ_N (day^{-1})	15.0	15.0	15.0	15.0	15.0	15.0
	Level					
	13	14	15	16	17	
σ	0.105	0.0655	0.0371	0.0191	0.00908	
T_0 (K)	211.4	214.7	219.5	226.4	236.7	
ΔT (K)	0.0	0.0	0.0	0.0	0.0	
τ_N (day^{-1})	15.0	15.0	10.0	6.52	3.93	
	Level					
	18		19		20	
σ	0.00374		0.00148		0.000415	
T_0 (K)	254.1		282.2		356.5	
ΔT (K)	0.0		0.0		0.0	
τ_N (day^{-1})	2.2		1.61		1.5	

The model has a heating term that is represented by the Newtonian forcing toward the prescribed equilibrium temperature T^* given by

$$T^* = T_0(\sigma) + \frac{\Delta T(\sigma)}{2}\left(\cos 2\phi - \frac{1}{3}\right), \qquad (1)$$

where ϕ is latitude, $T_0(\sigma)$ is the global mean temperature at each level, and $\Delta T(\sigma)$ is the pole to equator temperature difference. This is a simple representation of an equinox condition often adopted in simplified theoretical models (e.g., Held and Hou 1980; Yu and Hartmann 1993). The values of $T_0(\sigma)$ and $\Delta T(\sigma)$ are listed in Table 1; T_0 is determined to set the mean Brunt–Väisälä frequency N to 1.14×10^{-2} s^{-1} in the troposphere and to 2.24×10^{-2} s^{-1} in the stratosphere. The relaxation time for the Newtonian heating τ_N is also listed in Table 1; $\tau_N = 15.0$ days for most levels and smaller values for sponge layers.

The model has no moist processes and contains only the dry convective adjustment. Internal horizontal dissipation in the form ∇^4 is applied to temperature, vorticity, and divergence equations with the damping time of 6 h for the maximum wavenumber 42. No mountains are included in the both hemispheres. The surface friction is parameterized by the Rayleigh friction at the bottom level following James and James (1992) with a relaxation time of $\tau_R = 0.5$ day for the control run and

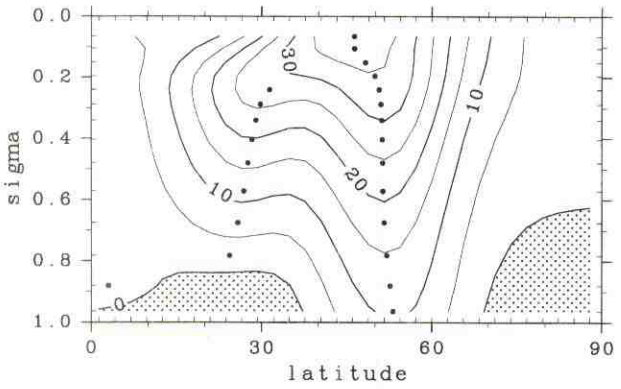

FIG. 1. Latitude–height section of the time and zonal-mean zonal flow. Contour interval is 5 m s^{-1}. Easterlies are shaded and the local maximum on each level is denoted by a dot.

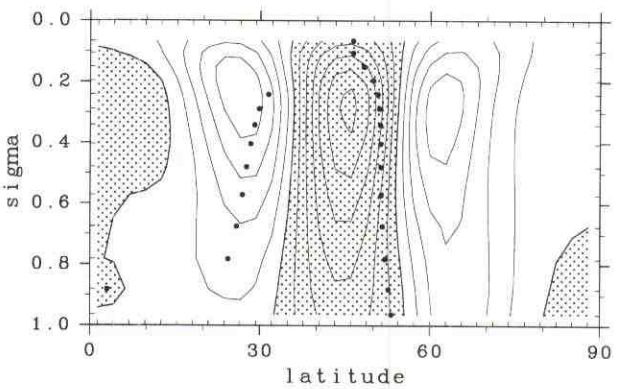

FIG. 2. Latitude–height section of the EOF1 mode of zonal mean zonal flow variations. Negative values are shaded and contour interval is 0.02.

τ_R = 1.0 day and 0.25 day for experimental runs. Note that the surface friction in the control run gives realistic behavior of a model atmosphere as described by James (1994, section 2.5), although he and his coworkers applied the relaxation time of 1 day because of a lower vertical resolution (five equally spaced σ levels) of their model. The heat flux across the bottom boundary is not included.

The initial state is a zonally symmetric state with a small disturbance; temperature is set to T^* and zonal flow is balanced to the temperature field, assuming no surface wind. An initial disturbance is added to the surface pressure field with a Gaussian form; the maximum value is 10 hPa at 5°N, 180°E with the e-folding length of 10°. This asymmetry of the initial disturbance with respect to the equator causes different evolutions between the two hemispheres.

Integrations are performed for 3180 days for all the runs by means of the semi-implicit method. For the first 1500 days, a coarse resolution of T21 is used with a 60-min time step to save computation time for the initial transient period. A transient period of 400 days after the increase of resolution to T42 with a 30-min time step is also discarded. Therefore the analyzed period is the last 1281 days of the integration with a sampling interval of one day. Since the evolutions in both hemispheres are fundamentally independent of each other, data in the Southern Hemisphere are transformed to those in the coordinates of the Northern Hemisphere. In this way, we deal with them as if there were two Northern Hemisphere datasets, although the notations of "Northern" and "Southern" only mean $\phi > 0$ and $\phi < 0$, respectively, because of the symmetric external conditions with respect to the equator.

3. The control run

a. *Vacillations of the mean zonal flow*

A latitude–height section of the time-averaged zonal mean zonal flow is shown in Fig. 1, which is obtained from the two hemispheric datasets and is quite similar to those obtained from either dataset. There is a strong westerly jet in midlatitudes with a maximum wind speed of 37 m s^{-1} near the tropopause. The subtropical jet in the upper troposphere is rather weak. The surface easterlies exist in low latitudes and in high latitudes.

An EOF analysis is applied to the time series of the mean zonal flow to determine the most significant structure in the fluctuations. The EOF1 mode, which explains more than 44% of the variance, is illustrated in Fig. 2. It shows nearly barotropic structure with three extrema of alternating sign centered at ϕ = 27°, 46°, and 63° near the tropopause.

These characteristics of the climatology and variation of the mean zonal flow have been observed in the Southern Hemisphere (Yoden et al. 1987; Hartmann 1995) and in the numerical experiments (James and James 1992; Yu and Hartmann 1993). However, the numerical results of James and James (1992) and ours show stronger fluctuations near the tropopause than the others. These may be caused by the parameterizations of the surface friction and the vertical diffusion.

The principal component of the EOF1 mode (hereafter PC1) is shown in Fig. 3. A power spectral analysis shows that the significant periods of fluctuations are between 80 and 150 days, although the variations are considerably irregular with a red-noise background spectrum. Note that the correlation of the PC1s of the two hemisphere datasets (a) and (b) is 0.12 without strong interhemispheric relation in the zonal flow vacillation.

b. *Two extreme phases of the vacillation*

The relationship between the mean zonal flow and baroclinic eddies is investigated in detail for the two most extreme phases of the PC1 variation. As shown in Fig. 3, the positive extreme (hereafter $U+$) is from day 2440 to day 2445 of the Northern Hemisphere and the negative extreme (hereafter $U-$) is from day 1920 to day 1925 of the Southern Hemisphere.

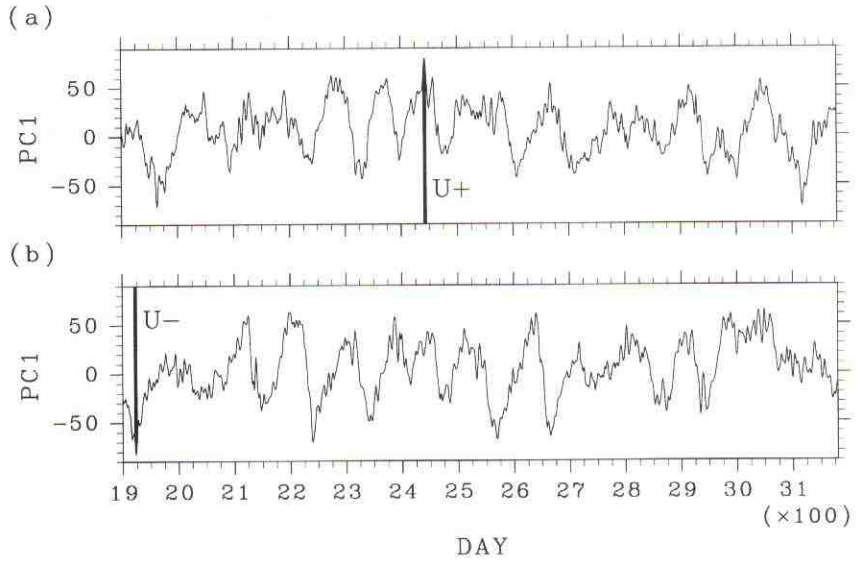

FIG. 3. Principal component of the EOF1 mode (PC1) for (a) the Northern Hemisphere dataset and (b) the Southern Hemisphere dataset.

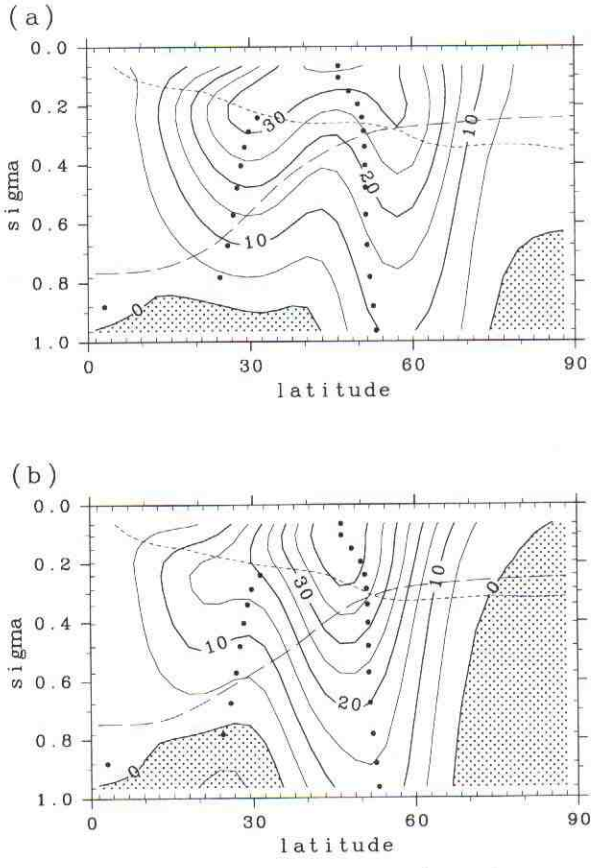

FIG. 4. Latitude–height sections of the composite zonal mean zonal flow in (a) the $U+$ period and (b) the $U-$ period. Zonal mean of PV = 2 PVU surface (broken line) and θ = 310 K isentropic surface (dashed line) are also shown. Dots represent the local maximum of the climatological jet (same as Fig. 1).

Figure 4 illustrates the composite of the zonal-mean zonal flow during these two periods. In the $U+$ period (Fig. 4a), there are two zonal-mean jet streams near the tropopause; one at $\phi = 58°$ and the other at $\phi = 30°$. In this figure the broken line shows PV = 2 PVU (potential vorticity unit $\equiv 10^{-6}$ m^2 s^{-1} K kg^{-1}) level, which is a good approximation of the tropopause. Note that the main higher-latitude jet, which is closely related to the behavior of midlatitude cyclones, shifts 7° poleward from the time-averaged state (dots in Fig. 4a). In the $U-$ period (Fig. 4b), on the other hand, there is a narrow jet stream located at $\phi = 48° \sim 50°$, which is 5° equatorward from the time-averaged state. The subtropical jet near $\phi = 25°$ is very weak. Examining the zonal-mean zonal flow profiles averaged on the θ = 310 K isentropic surface (dashed line in Fig. 4), which will be investigated in section 5 (Fig. 16), we see a dominant local maximum of 30 m s^{-1} exists at $\phi = 58°$ in the $U+$ period, while the maximum of 37 m s^{-1} exists at $\phi = 48°$ in the $U-$ period. These profiles are qualitatively similar to those in the observational study by Hartmann (1995), although the maximum wind speeds in his two composites are nearly equal to each other.

A PV–θ analysis (Hoskins et al. 1985) is performed to diagnose the evolution of baroclinic eddies in the two most extreme periods. Although THM diagnosed isentropic contours on the PV = 2 PVU surface, which is a good approximation of the tropopause, we analyzed PV contours on the θ = 310 K isentropic surface following Hartmann (1995). These two surfaces are shown in Fig. 4 by a broken line (PV) and a dashed line (θ).

Figure 5 shows the daily sequence of PV contours and the horizontal flow field on the θ = 310 K isentropic

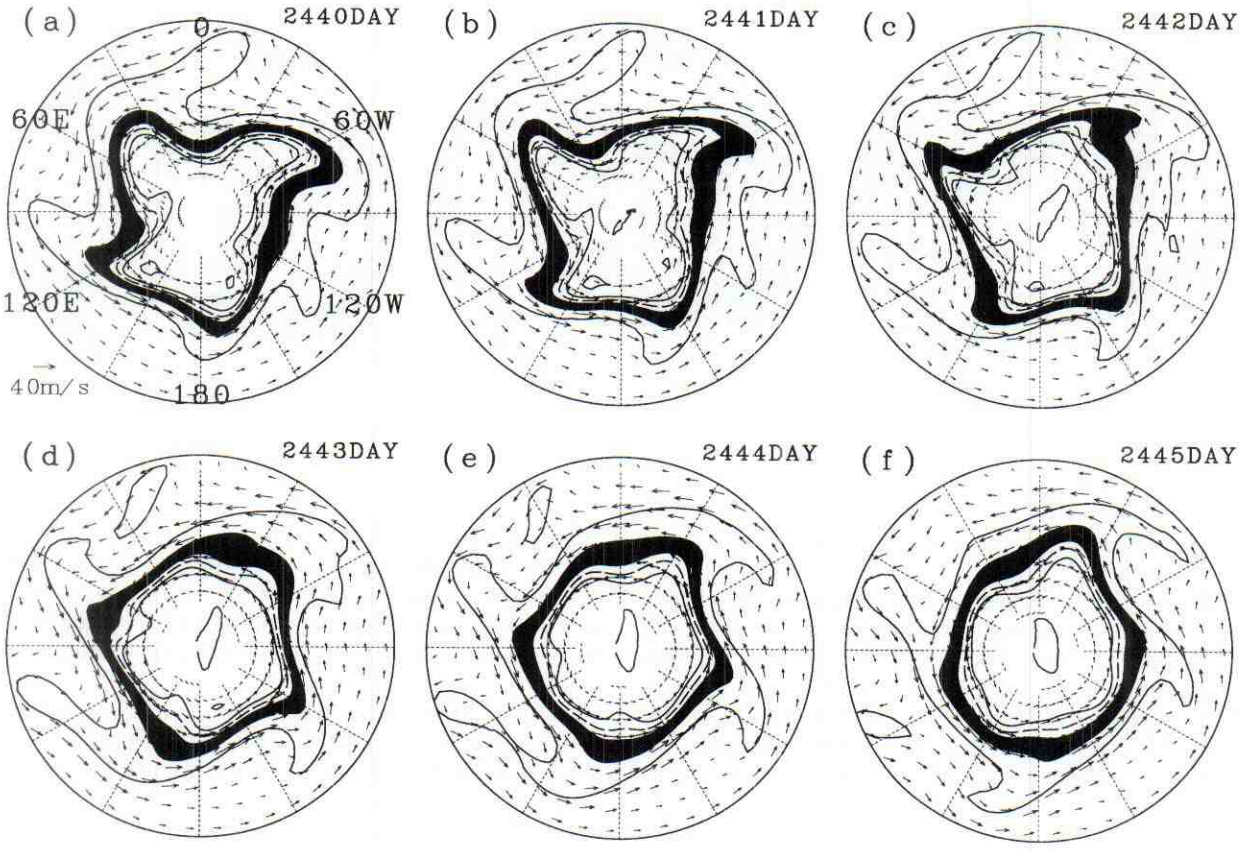

FIG. 5. PV on the θ = 310 K isentropic surface in the $U+$ period. Contour interval is 1 PVU and 3.5 PVU contour is a dashed line. Regions between 2 and 3 PVU are blacked out. Horizontal flow vectors more than 5 m s^{-1} are also shown. Unit vector in (a) is 40 m s^{-1}. Polar stereo projection is used. The boundary circle is 30°N. Lines of meridians and parallels are drawn for every 30°.

surface during the $U+$ period. Most of the baroclinic eddies in midlatitudes are characterized by the anticyclonic behavior. High PV air parcels are anticyclonically advected equatorward and PV contours show a pattern of Rossby wave breaking familiar in the winter stratosphere. For example, a streamer of 1 PVU contour around 100°E on day 2440 (Fig. 5a), which tilts backward with northeast–southwest orientation, continues to be elongated and thinned due to some cross-contour flow associated with the anticyclone in the rear of the trough (Figs. 5b–d). A strong cyclonic circulation around the tip of the PV streamer on day 2444 (Fig. 5e) is indicative of a secondary instability. Finally the streamer is pinched out backward by day 2445 (Fig. 5f). Some weak cyclonic breakings on the poleward side of the jet are also perceptible; a 4 PVU contour shows a cyclonic wrapping-up process around 60°E on day 2440.

Temperature near the surface is shown in Fig. 6 for the first 3 days of the $U+$ period. Cold fronts are discernible as a band of large gradient of temperature under the leading edge of the corresponding upper trough. A large meander of the cold front around 20°E on day 2442 is suggestive of a secondary instability of the frontal system, interacting with the upper westward PV streamer above it (Thorncroft and Hoskins 1990). A surface pressure anomaly associated with this instability is depressed at the rate of 2 hPa a day from day 2440 to day 2443.

During the $U-$ period, evolutions of the PV contours are characterized by notable cyclonic breakings on the poleward side of the mean jet (Fig. 7). On day 1920 (Fig. 7a), there are four vigorous troughs and that around 45°E is in a mature stage with a wrapping-up pattern of high and low PV air parcels. By day 1922, significant homogenization is in progress but there still remains a cutoff of low PV in high latitudes, which disappears 1 day after (Fig. 7d). After day 1922, the trough becomes thinner owing to the anticyclonic breaking (Figs. 7d–f), although it is rather exceptional event in this period. Another notable cyclonic breaking is seen around 30°E on day 1925.

The corresponding temperature field near the surface (Fig. 8) shows warm fronts and bent-back structures as well as cold fronts (around 90°E and 120°W on day 1920). These warm fronts are linked to the intrusion of low PV air into high latitudes in the upper troposphere (Fig. 7a). Comparing the surface frontal systems between the $U+$ and $U-$ periods, we notice the sharpness of warm fronts in the $U-$ period. Such a sharp warm front is formed by a strong circulation near the surface

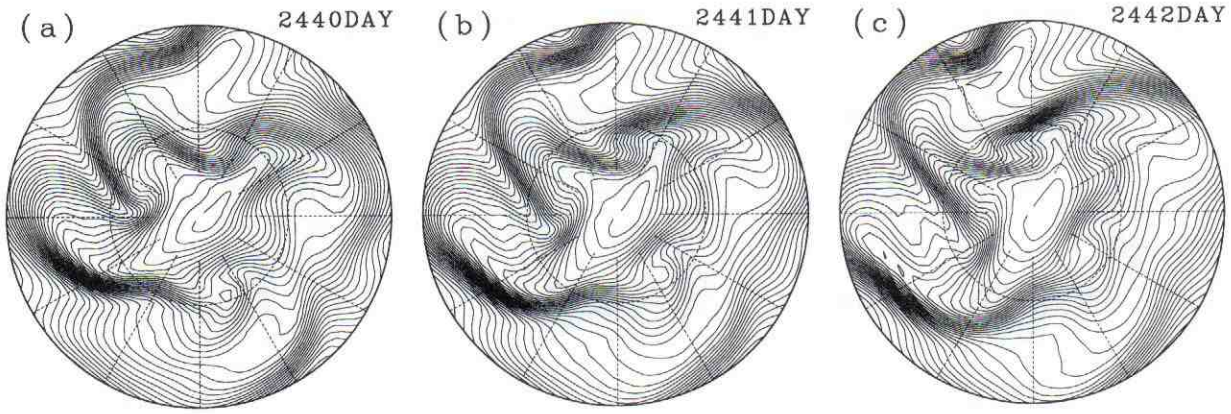

FIG. 6. Temperature on $\sigma = 0.963$ surface for the first 3 days of the $U+$ period. Contour interval is 1 K. The map projection is the same as in Fig. 5.

that is induced by a large mass of high PV air above the system.

These synoptic properties are similar to the characteristics of the nonlinear development in the life cycle experiments of baroclinic waves (THM). Most cyclones in the $U+$ period correspond to the LC1 type, showing the anticyclonic breaking, and those in the $U-$ period to the LC2 type, showing the cyclonic breaking, respectively, although cyclones in the $U-$ period decay rather rapidly as was pointed by Lee and Feldstein (1996). Thus, the basic features of the PV evolutions related to the zonal flow vacillation, which was observed in the Southern Hemisphere winter by Hartmann (1995), are well simulated in our idealized global circulation model.

In order to get quantitative information on the baroclinic eddy activity during these extreme periods, zonal-mean eddy kinetic energy (EKE), defined as $(\overline{u'^2} +$

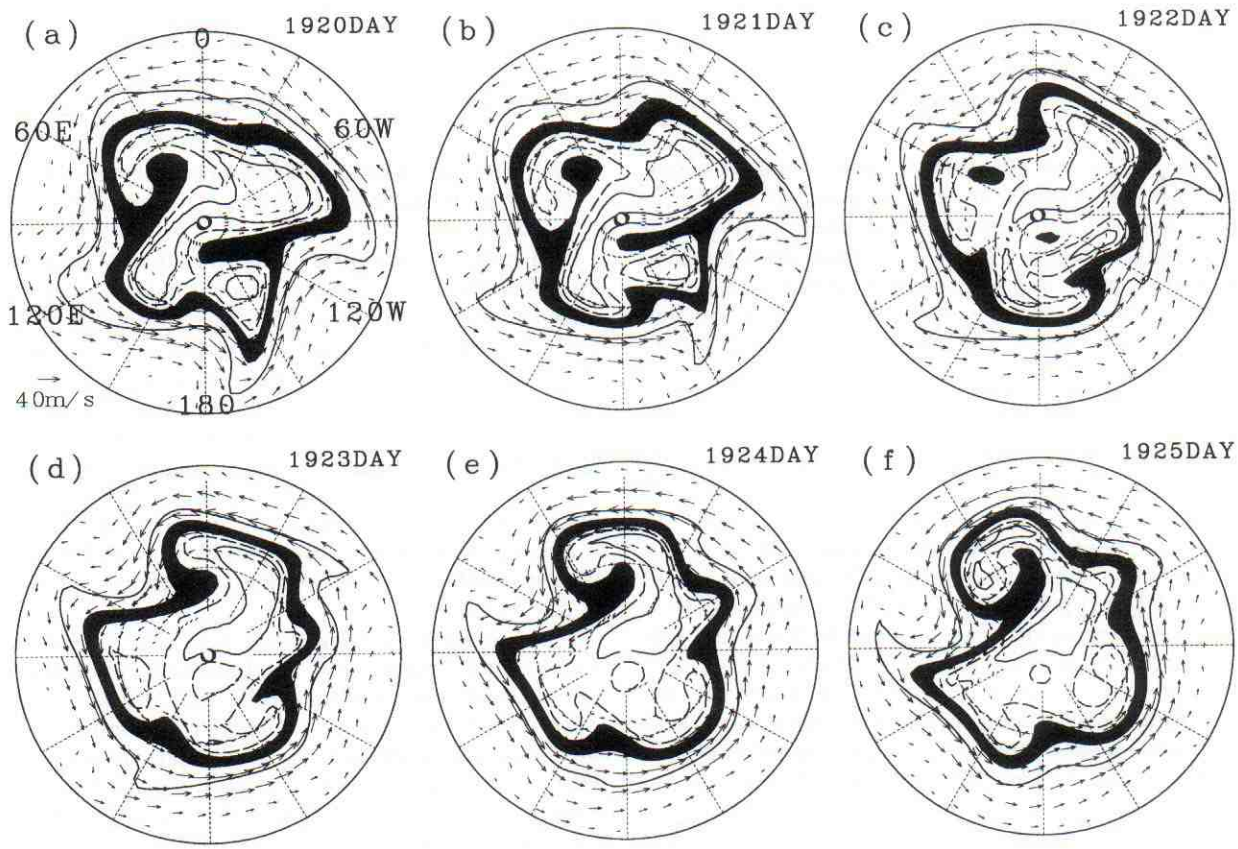

FIG. 7. As in Fig. 5 but for the $U-$ period.

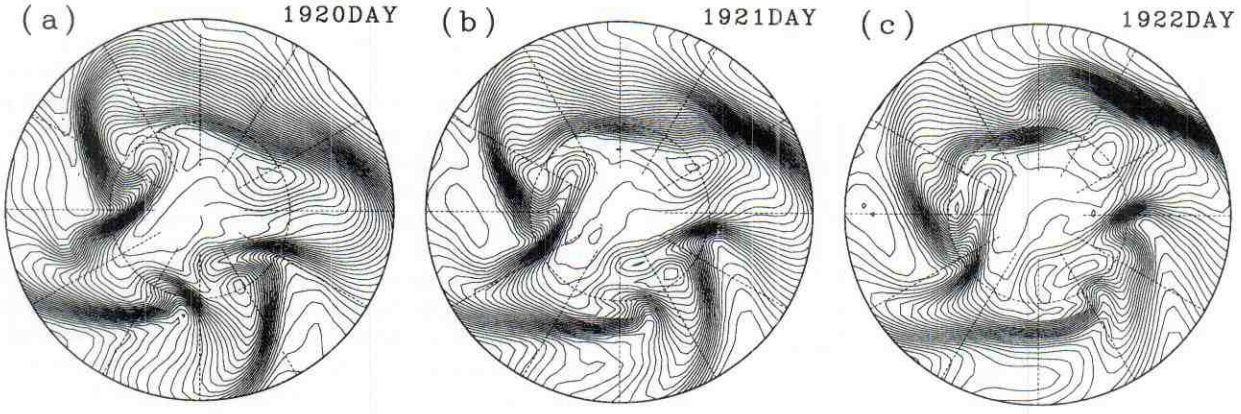

FIG. 8. As in Fig. 6 but for the first 3 days of the $U-$ period.

$\overline{v'^2})/2$, is computed, where u is the zonal wind, v the meridional wind, overbar ($\bar{}$) the zonal mean, and prime ($'$) deviation from the zonal mean. Figure 9 shows meridional cross sections of EKE averaged for the two periods of $U+$ and $U-$. In both periods, the averaged EKE is large in the upper troposphere and has a maximum near the main high-latitude jet: $\phi = 55°$ for the $U+$ period and 43° for the $U-$ period. The maximum value in the $U-$ period is 2.2 times larger than that in the $U+$ period. In the $U+$ period, the EKE is larger in the equatorward side of the main jet, and contours in the upper troposphere have a lobe in mid- and low latitudes where the streamers are frequently formed. On the other hand, a lobe of large EKE is also seen in the poleward side of the main jet in the $U-$ period consistent with the wrapping-up processes in high latitudes.

c. *Statistical relationship*

To obtain a statistical relationship between the zonal flow vacillation and the morphology of the life cycles of baroclinic eddies for the entire period analyzed, we introduce a primitive index by which we can distinguish the difference of breaking patterns. Figure 10 shows the procedure to obtain the index as a representative latitude of wave-breaking regions for some examples of the $U+$ and $U-$ periods. First, the latitudinal band that is between the most equatorward contour of 1 PVU and the most poleward contour of 3.5 PVU for each longitude is chosen; the other regions are blacked out in Fig. 10. Next, negative regions of the meridional gradient of PV are contoured and positive regions are excluded by shading. Since the negative regions correspond to wave-breaking regions, an averaged latitude of these regions with the weight of the negative PV gradient is used as the definition of the index, which is called LC index hereafter. The LC index is 47.3°, 47.0°, and 45.4°, respectively, for the first 3 days of the $U+$ period shown in Figs. 10a–c, while it is 67.2°, 66.8°, and 65.5°, respectively, for the $U-$ period (Figs. 10d–f). The LC index is low for the LC1-type anticyclonic breakings and high for the LC2-type cyclonic breakings. The LC index has no value for days at which no negative region of the PV gradients exists (23 days out of 2562 days). Note that widespread equatorward breaking regions for the $U-$ periods as well as for the $U+$ periods are excluded by the lower PV boundary, because these areas with sparse PV contours are not only less important for the dynamics of cyclones but also rather asynchronous to midlatitude cyclones; perturbations of low PV contours fade out more slowly in low latitudes by the Newtonian forcing and the internal dissipation.

Evolution of the LC index is illustrated in Fig. 11 for all the analyzed period. The correlation coefficient between the LC index and PC1 shown in Fig. 3 is −0.61. When PC1 has a positively large value, the LC index tends to have a small value. For example, the LC index is persistently small for the periods of days 2270–2300, days 2350–2380, and days 2420–2460 in Fig. 11a, during which PC1 is also positively large. On the other hand, the LC index is persistently large in the periods of days 1940–1980, days 2320–2340, and days 3100–3130 in Fig. 11a, during which PC1 is negatively large. When PC1 has a small value near zero, the LC index tends to fluctuate from one extreme to the other intermittently, because it directly reflects several small breaking regions during such periods. Some examples are the periods of days 1950–2080, days 2700–2780, and days 3070–3190 in Fig. 11b.

A scatter diagram as well as histograms of the LC index and PC1 is shown in Fig. 12. There are two dominant clusters in this scatter diagram; one is in positive PC1 and low LC-index area and the other in negative PC1 and high LC-index area. The histograms of the LC index (upper panel) show a clear bimodal distribution with maxima around 45° and 65°, while that of PC1 shows a unimodal Gaussian-like distribution. Thus, the two breaking patterns as described in the previous subsection are frequently observed alternatively with a negative correlation to PC1, an index of the zonal flow vacillation. Although the definition of the LC index contains some arbitrary parameters, the bimodality is a ro-

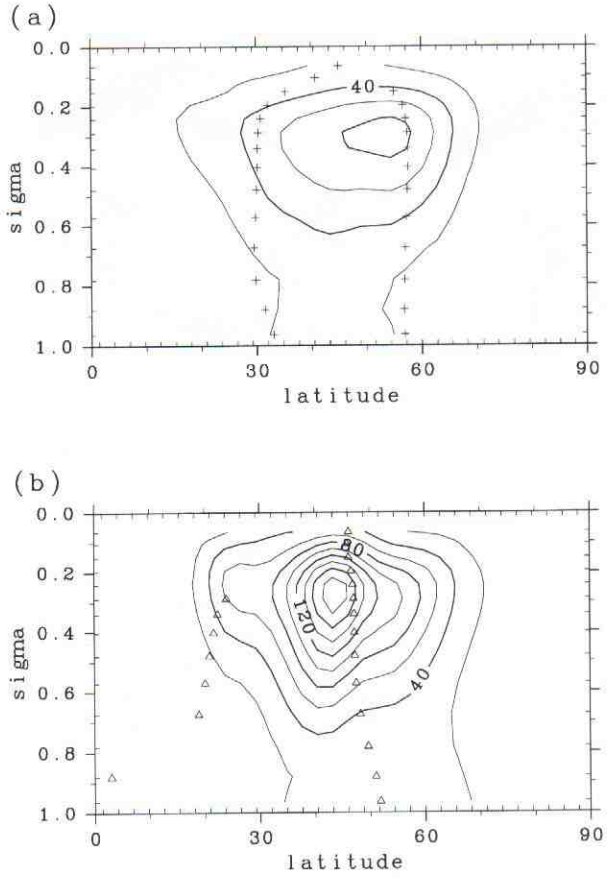

FIG. 9. Latitude–height sections of composite zonal-mean eddy kinetic energy in (a) the $U+$ period and (b) the $U-$ period. Contour interval is 10 $m^2 s^{-2}$. Symbols + in (a) and △ in (b) indicate the axis of the jets in Fig. 4a and 4b, respectively.

bust feature insensitive to the choice of PV contours; for example, it is still obtained for 0.75 PVU or 1.25 PVU instead of 1.0 PVU.

4. Experimental runs

Two experimental runs are performed to obtain a deeper insight about the relationship between the mean zonal flow and baroclinic eddy life cycles. Since the latitude of the climatological jets depends on the intensity of surface drag in the longtime integrations by James and Gray (1986, their Figs. 2 and 6), we perform two experiments in which the timescale of the Rayleigh friction τ_R is doubled (τ_R = 1.0 day) or halved (0.25 day). The time-averaged zonal-mean zonal flows are shown in Fig. 13. A notable difference between these two runs is a barotropic component centered at 62°; the mean zonal flow in the low-drag run (Fig. 13a) is stronger by about 10 m s^{-1} than that in the high-drag run (Fig. 13b). For the low-drag run, the main higher-latitude jet is located in higher latitudes of 3° ~ 5° compared with that of the control run (dots in Fig. 13), while the main jet for the high-drag run shifts 3° ~ 4° equatorward from the control run. These characters are consistent with James and Gray (1986). Position of the main jet for the low-drag run is close to that in the $U+$ period (Fig. 4a) of the control run and that for the high-drag run is similar to the $U-$ period (Fig. 4b).

In order to investigate the relationship between the mean zonal flow and the morphology of the life cycles for these experimental runs, the LC index is computed. Since PC1 used in the previous section is not appropriate as a common measure to characterize the mean zonal flow, we adopt the latitude of the maximum zonal-mean flow on the θ = 310 K isentropic surface as a measure for the zonal-mean jet. Scatter diagrams of this latitude versus the LC index are shown in Fig. 14. For the control run (Fig. 14b), the two-dimensional distribution is quite similar to Fig. 12 because the correlation between PC1 and the latitude of the zonal-mean jet is more than 0.88. For the low-drag run (Fig. 14a), the latitude of the zonal-mean jet varies widely, but a cluster is prominent for some low values of the LC index, corresponding to one of the two clusters in the control run. It is indicative of frequent emergence of the LC1-type anticyclonic breakings. For the high-drag runs (Fig. 14c), on the other hand, a cluster corresponding to the other cluster in the control run is remarkable; it is indicative of the dominance of the LC2-type cyclonic breakings.

Histograms of the LC index and the latitude of the maximum zonal-mean flow are shown in Fig. 15 for these runs. The LC index for the low-drag run (thick broken line) has a peak around 45° where the control run (thin solid line) has one of two peaks. On the other hand, that for the high-drag run (thick solid line) has a peak around 63° where the control run has the other peak. The latitude of the maximum zonal-mean flow shows basically unimodal distribution for all the three runs, of which peak shifts poleward for the low-drag run and equatorward for the high-drag run.

5. Discussion

Two experimental runs in the previous section support the relationship between the mean zonal flow and baroclinic eddies obtained in the control run. The LC1-type anticyclonic breakings are frequently observed in the low-drag run in which the zonal-mean jet is located in higher latitudes, while the LC-2 type cyclonic breakings are frequently observed in the high-drag run with the zonal-mean jet in lower latitudes. However, bimodality of the LC index (or the breaking pattern of upper-air troughs) is obtained only in the control run with a medium value of the surface drag. From these results we can imagine the following picture of the "bifurcation" of flow regimes: when the bifurcation parameter, the relaxation time of the Rayleigh friction τ_R, is large enough, one flow regime (or strange attractor) corresponding to the high-latitude jet with anticyclonic breakings is realized in longtime integrations. On the other hand, another regime corresponding to the low-

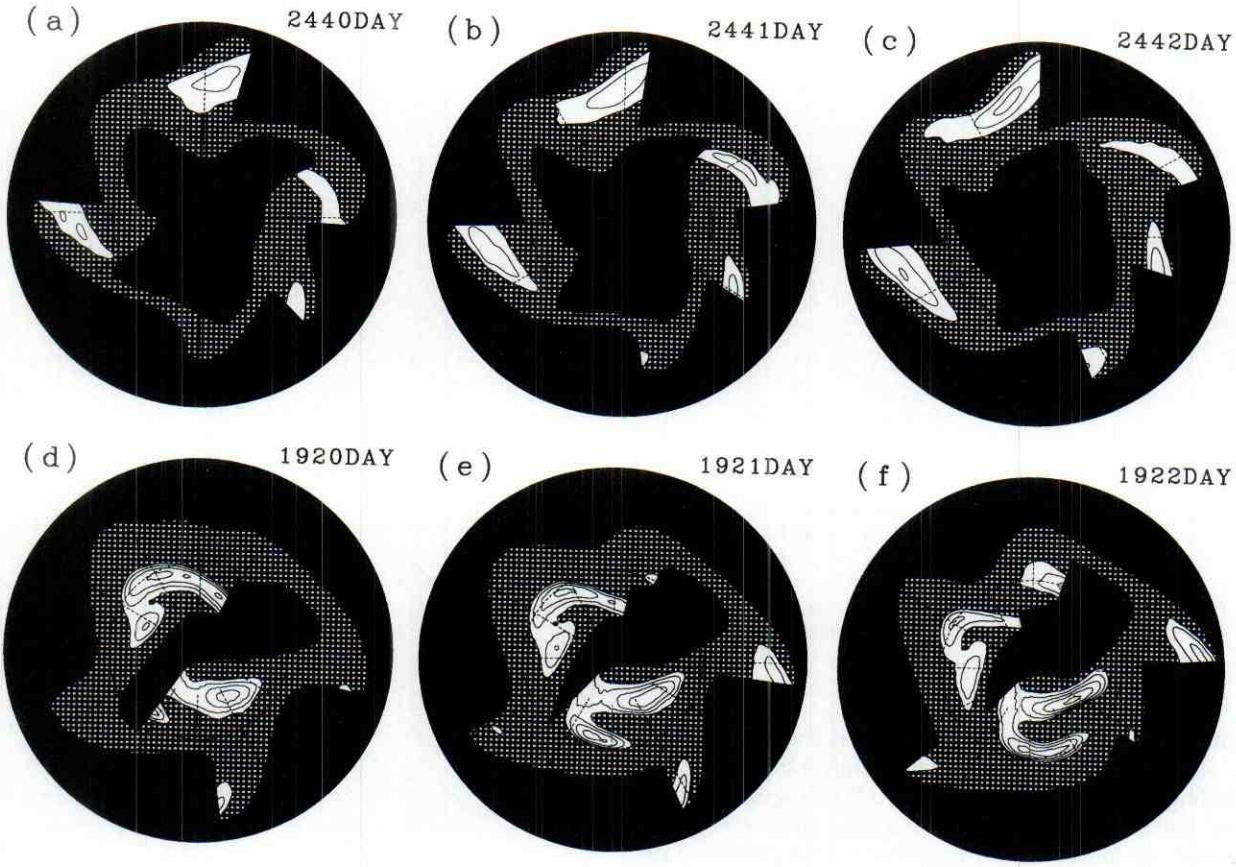

FIG. 10. Definition of the LC index. Negative regions of the meridional PV gradient on the 310-K isentropic surface are contoured for the first 3 days of the $U+$ period (a–c) and the $U-$ period (d–f). Contour interval is 5×10^{-6} PVU m^{-1}. See text for details.

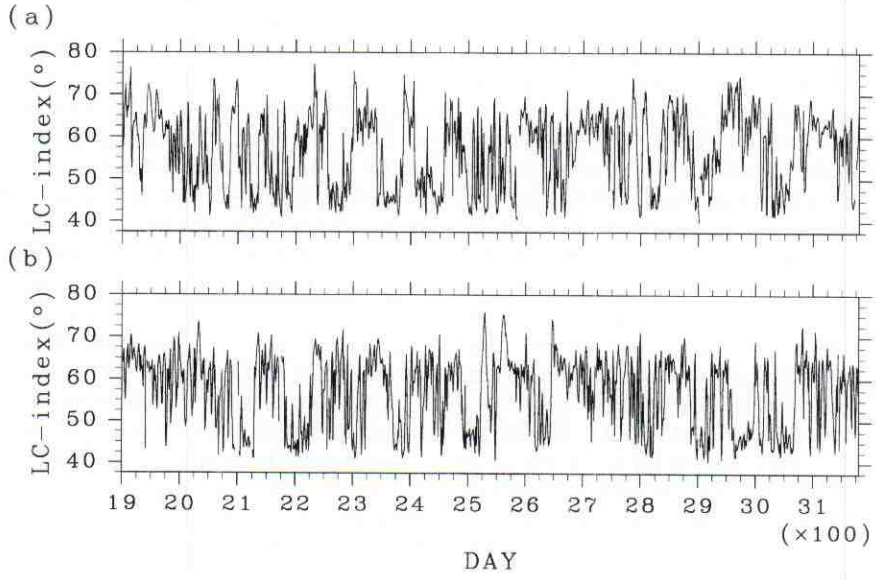

FIG. 11. As in Fig. 3 but for the LC index.

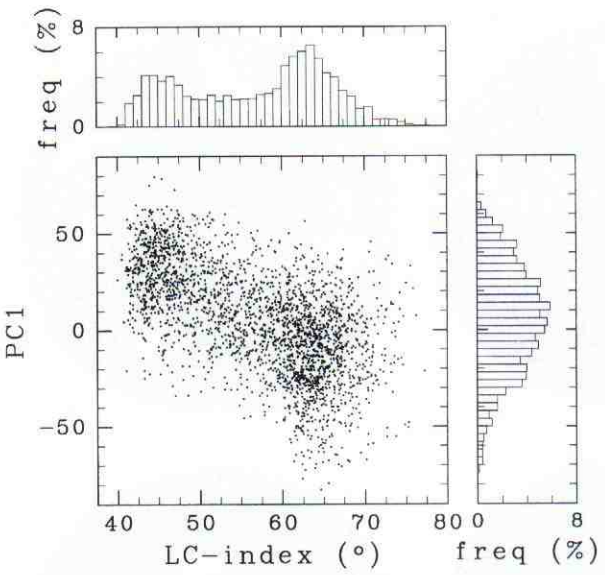

FIG. 12. Scatter diagram of the full dataset on the LC index–PC1 plane. Upper panel and right panel are one-dimensional distribution of the LC index and PC1, respectively.

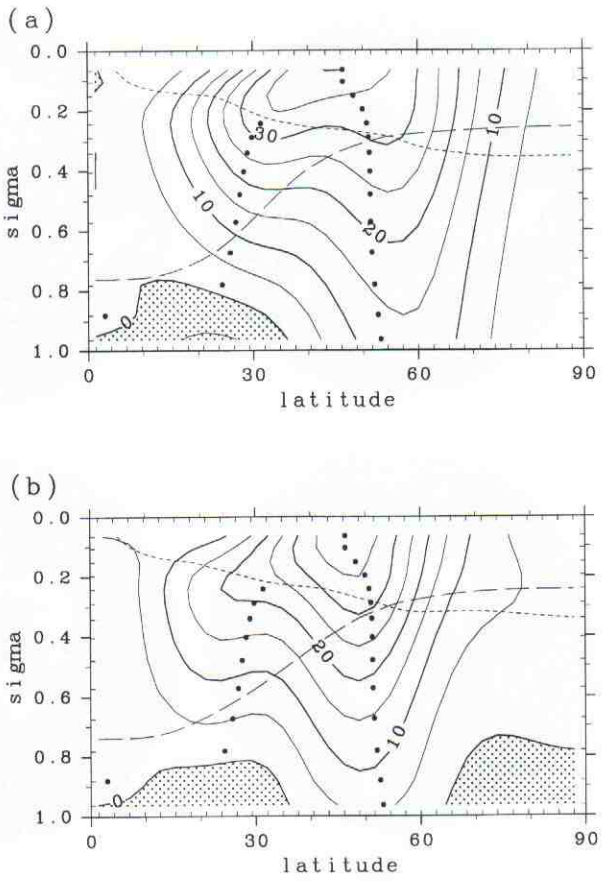

FIG. 13. As in Fig. 1 but for (a) τ_R = 1.0 day and (b) τ_R = 0.25 day. Dots represent the local maximum of the zonal-mean zonal flow for the control run of τ_R = 0.5 day (same as Fig. 1). Zonal mean of PV = 2 PVU surface (broken line) and θ = 310 K isentropic surface (dashed line) are also shown.

latitude jet with cyclonic breakings is realized when τ_R is small enough. For an intermediate range of τ_R including the control run, these two flow regimes coexist and both of the regimes are realized alternatively and irregularly in long time integrations. This picture of the persistence of multiple flow regimes and irregular transitions between them due to internal dynamics is a familiar paradigm of a nonlinear atmospheric circulation system since the pioneering work by Charney and DeVore (1979).

Two breaking patterns of baroclinic eddies, which are obtained in the present longtime integrations of a forced-dissipative system with the Newtonian forcing, Rayleigh friction, and internal dissipations, are basically formed by the same process as the two paradigms of baroclinic wave life cycles obtained in the one-shot experiments of a conservative system with neither forcing nor frictional dissipation (THM). The position of the zonal-mean jet in the meridional section is the most important factor that determines the breaking pattern. The anticyclonic shear on the equatorward flank of the high-latitude jet is responsible for the anticyclonic breaking, while the cyclonic shear on the poleward flank of the low-latitude jet is responsible for the cyclonic breaking. However, we can also point out some differences between the present longtime integrations and the one-shot experiments. The persistence of the cyclonic breakings is a notable example; the large-scale vortices resulting from the cyclonic wrapping-up process in the present study decay within a few days, as shown in Fig. 7, while those in the one-shot experiment have a decaying timescale of 10 days. The relative location of the latitude of maximum EKE from the zonal-mean jet is also different between the present study and the one-shot experiments. In the one-shot experiments, the maximum of EKE exists on the equatorward flank of the zonal-mean jet in LC1, while it exists on the poleward flank in LC2. In the present longtime integrations, on the other hand, the maximum of EKE is close to the zonal-mean jet for the two extreme periods of the control run, as shown in Fig. 9. A quite similar relationship is also confirmed by compositing the EKE and the mean zonal flow for the period during which the PC1 is above (below) 1.5 standard deviation for the positive (negative) value.

The LC index, which is an averaged latitude of the breaking regions, was introduced as a measure to characterize the breaking patterns of the upper-air troughs. It was useful for distinguishing the breaking patterns associated with the variations of mean zonal flow. We expect that this index is also useful for a quantitative diagnosis of the series of synoptic maps in the Southern Hemisphere as those analyzed by Hartmann (1995), because his analysis of PV patterns shows predominance of one of the two breaking patterns in each extreme phase of the zonal flow vacillation. However, the

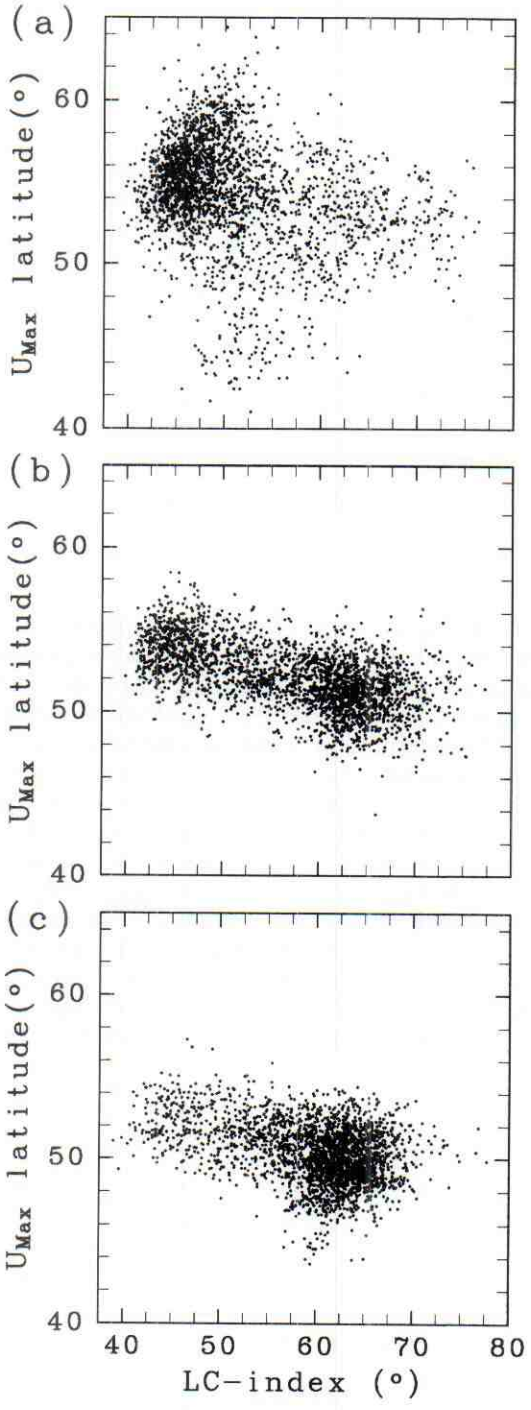

FIG. 14. Scatter diagrams of the latitude of the maximum zonal mean zonal flow on the 310-K isentropic surface and the LC index for (a) τ_R = 1.0 day, (b) τ_R = 0.5 day, and (c) τ_R = 0.25 day.

averaged latitude of the breaking regions may have some limitation for application to the Northern Hemisphere, because it is rather common that two types of breaking patterns are observed simultaneously in different longitudes in the Northern Hemisphere. Some other quantities on the distribution of breaking regions may be necessary for a quantitative diagnosis in the Northern Hemisphere.

In order to clarify the deformation field of the 310-K isentropic surface, we investigate a two-dimensional velocity gradient $\mathbf{L}$ given by

$$\mathbf{L}(u, v) \equiv \frac{1}{a}\begin{pmatrix} \dfrac{1}{\cos\phi}\left(\dfrac{\partial u}{\partial \lambda} - v\sin\phi\right) & \dfrac{1}{\cos\phi}\left(\dfrac{\partial v}{\partial \lambda} + u\sin\phi\right) \\ \dfrac{\partial u}{\partial \phi} & \dfrac{\partial v}{\partial \phi} \end{pmatrix}, \tag{2}$$

where u and v are the zonal and meridional wind, respectively, on the 310-K isentropic surface; λ is longitude; ϕ is latitude; and a is the radius of the earth.

The velocity gradient tensor $\mathbf{L}$ is divided into symmetric ($\mathbf{L}_s$) and antisymmetric ($\mathbf{L}_a$) parts; the former is called the rate of strain (e.g., Batchelor 1967). A scalar magnitude of the rate of strain is given by $S(u, v) = |\mathbf{L}_s| = [\mathrm{tr}(\mathbf{L}_s\mathbf{L}_s^T)]^{1/2}$. Nakamura and Plumb (1994) investigated breaking patterns of Rossby waves superposed on some idealized circular vortices and analyzed the radial distribution of the magnitude of strain for each vortex to characterize the breaking patterns. In this study we calculated the magnitude of strain for the mean zonal flow on the 310-K isentropic surface:

$$S(\bar{u}, 0) = \frac{1}{2^{1/2}a}\left|\frac{\partial \bar{u}}{\partial \phi} + \bar{u}\tan\phi\right|. \tag{3}$$

Figure 16 shows the meridional distribution of S as well as $\bar{u}$ for the composite field during the two extreme phases of the vacillation, $U+$ and $U-$, analyzed in section 3b. For the $U+$ period (Fig. 16a), the strain is largest on the equatorward flank of the mean zonal jet and PV $\simeq$ 1.5 PVU in the high-strain latitudes. These are consistent with the characteristics of anticyclonic breakings during this period; the breaking pattern is most discernible for the contours of 1 $\sim$ 2 PVU on the equatorward side of the zonal-mean jet (Fig. 5). For the $U-$ period (Fig. 16b), on the other hand, the strain has a local maximum on the poleward flank of the zonal-mean jet where PV $\simeq$ 3 PVU, consistent with the cyclonic breaking patterns (Fig. 7). Lower PV contours around another local maximum on the equatorward flank of the jet are less important for the dynamics of midlatitude cyclones as was noted in section 3c, although anticyclonic breakings corresponding to this maximum can also be interpreted through the rate of strain.

The velocity gradient tensor $\mathbf{L}(u, v)$ may be used to diagnose the evolution of breaking patterns on an isentropic surfaces. Since the character of the two-dimensional deformation field is given by the eigenvalues of $\mathbf{L}$, the discriminant Δ of the quadratic proper equation of $\mathbf{L}$ divides the flow field into stretching regions ($\Delta > 0$) and rotating regions ($\Delta < 0$; e.g., Ottino 1989). This measure of strain has been used

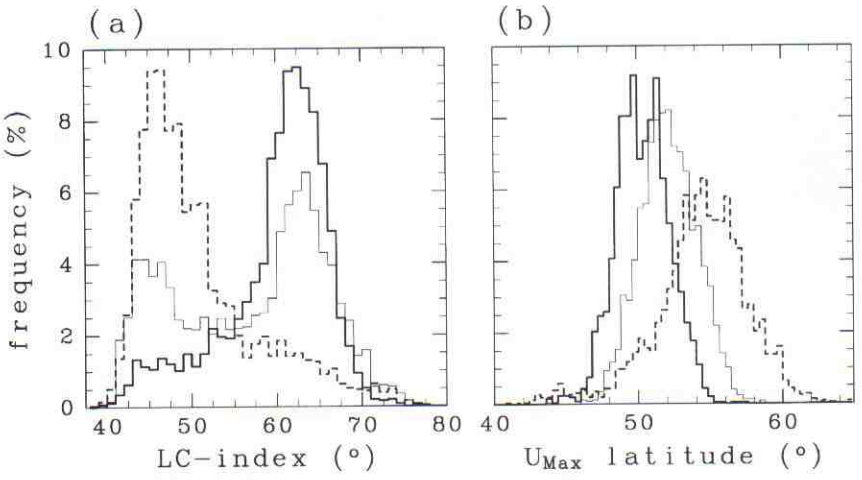

FIG. 15. Histograms of (a) the LC index and (b) the latitude of the maximum zonal-mean zonal flow on the 310-K isentropic surface. Thick broken line is for τ_R = 1.0 day, thin solid line for τ_R = 0.5 day, and thick solid line for τ_R = 0.25 day.

to analyze the flow field obtained in the numerical experiments on two-dimensional turbulence (e.g., Weiss 1991; Yoden and Yamada 1993). For the one-shot experiments such as Simmons and Hoskins (1980), it is confirmed that the spatial distribution of the measure is a useful tool to distinguish the tendency of breaking (not shown). However, it is not for the longtime integration experiments; clear relationship between the measure of strain and the breaking patterns is not obtained.

6. Conclusions

The relationship between the zonal flow vacillation and breaking patterns of baroclinic eddies was studied by integrating a simple global circulation model for a long period of over 3000 days under a perpetual equinox condition. An EOF analysis of the control run shows that the zonal flow vacillation is characterized by intermittent transitions between high-latitude and low-latitude jet regimes and that the barotropic shear of the westerly jet fluctuates predominantly as was pointed out in the previous studies. A PV–θ analysis during two extreme phases of the vacillations shows two typical evolutions of baroclinic eddies similar to the two paradigms of baroclinic wave life cycles (THM). In the period of high-latitude jet, life cycles of upper-air troughs are characterized by anticyclonic equatorward streamers of high PV air (i.e., anticyclonic breaking). In the period of low-

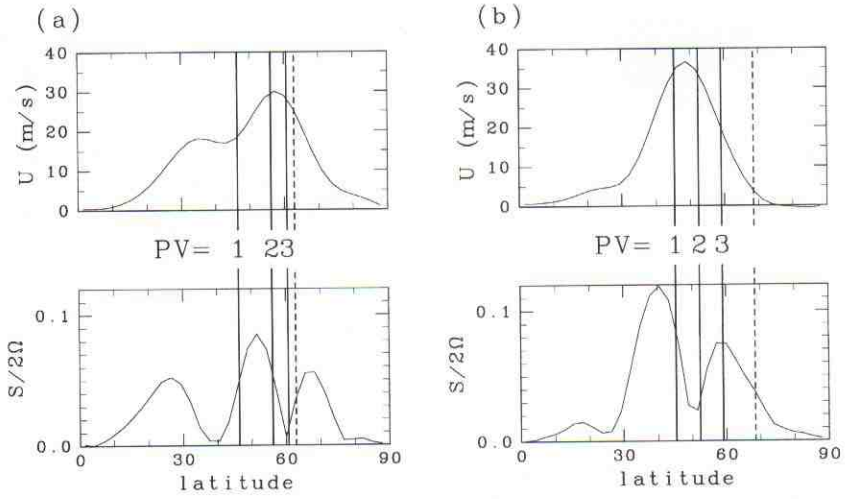

FIG. 16. Latitudinal profile of zonal-mean zonal flow (top) and dimensionless magnitude of strain $S/(2\Omega)$ (bottom), where Ω is the angular speed of the rotation of the earth. Location of zonal mean PVs are also shown by solid line (PV = 1, 2, and 3 PVU) and dashed line (PV = 3.5 PVU). Composites for (a) the $U+$ period and (b) the $U-$ period.

latitude jet, on the other hand, they are characterized by broadening troughs wrapping themselves up cyclonically (i.e., cyclonic breaking). These features obtained in our simple global circulation model are the counterpart of the observations in the Southern Hemisphere winter reported by Hartmann (1995). Furthermore, this relationship between the position of the zonal-mean jet and the breaking patterns of baroclinic eddies was confirmed throughout the entire period of 1281 days with the help of the LC index, which we defined as a typical latitude of wave breakings. The LC index indicates the bimodality of the wave breaking for the control run, although the position of the zonal-mean jet shows a unimodality of a Gaussian distribution.

Two experimental runs were performed in which the strength of the surface friction was varied. For the run with a halved surface drag, the zonal-mean jet is located climatologically in high latitudes because of the increase of the barotropic components of the zonal flow in high latitudes. The LC index shows a unimodal distribution around one of the two peaks in the control run, corresponding to anticyclonic breakings. For the run with a doubled surface drag, on the other hand, low-latitude jet and cyclonic breakings are predominant. When the surface drag is intermediate as the control run, one of the two patterns of the wave breakings emerge alternatively corresponding to the zonal flow variations generated in the model. These variations can be interpreted as the persistence and the transition between the two preferred flow regimes.

There are some differences in the wave breakings between the idealized one-shot experiments of baroclinic wave life cycles by THM and the present longtime integrations. For example, the pattern of cyclonic breakings decays more rapidly in the longtime integrations than in the one-shot experiments, as was pointed by Lee and Feldstein (1996). The relative location between the main zonal-mean jet and the latitude of the maximum EKE is also different; in the longtime integrations, the maximum EKE is usually located around the jet axis, while it is located on either side of the jet axis depending on the two paradigms of the life cycles in the one-shot experiments. These properties in the longtime integrations come from the variable interactions between finite-amplitude baroclinic eddies and the mean zonal flow. The complex deformation fields on the isentropic surface near the tropopause reflect this character of finite-amplitude disturbances.

Acknowledgments. The present numerical model and graphic tools were based on the codes in the GFD-DENNOU Library. Computations were performed on the KDK system at RASC, Kyoto University, and NEC SX-3/14R at the Computer Center of Osaka University. This work was supported in part by the Grant-in-Aid from the Ministry of Education, Science, Sports, and Culture of Japan, and by the Grant-in-Aid for the Cooperative Research with Center for Climate System Research, University of Tokyo.

REFERENCES

Appenzeller, C., and H. C. Davies, 1992: Structure of stratospheric intrusions into the troposphere. *Nature,* **358,** 570–572.

——, ——, and W. A. Norton, 1996: Fragmentation of stratospheric intrusions. *J. Geophys. Res.,* **101,** 1435–1456.

Batchelor, G. K., 1967: *An Introduction to Fluid Dynamics.* Cambridge University Press, 615 pp.

Charney, J. G., and J. G. DeVore, 1979: Multiple flow equilibria in the atmosphere and blocking. *J. Atmos. Sci.,* **36,** 1205–1216.

Hartmann, D. L., 1995: A PV view of zonal flow vacillation. *J. Atmos. Sci.,* **52,** 2561–2576.

——, and P. Zuercher, 1997: Response of baroclinic life cycles to barotropic shear. *J. Atmos. Sci.,* in press.

Held, I. M., and A. Y. Hou, 1980: Nonlinear axially symmetric circulations in a nearly inviscid atmosphere. *J. Atmos. Sci.,* **37,** 515–533.

Hoskins, B. J., M. E. McIntyre, and A. W. Robertson, 1985: On the use and significance of isentropic potential vorticity maps. *Quart. J. Roy. Meteor. Soc.,* **111,** 877–946.

James, I. N., 1994: *Introduction to Circulating Atmospheres.* Cambridge University Press, 422 pp.

——, and L. J. Gray, 1986: Concerning the effect of surface drag on the circulation of a baroclinic planetary atmosphere. *Quart. J. Roy. Meteor. Soc.,* **112,** 1231–1250.

——, and P. M. James, 1992: Spatial structure of ultra-low-frequency variability of the flow in a simple atmospheric circulation model. *Quart. J. Roy. Meteor. Soc.,* **118,** 1211–1233.

James, P. M., K. Fraedrich, and I. N. James, 1994: Wave-zonal-flow interaction and ultra-low-frequency variability in a simplified global circulation model. *Quart. J. Roy. Meteor. Soc.,* **120,** 1045–1067.

Karoly, D. J., 1990: The role of transient eddies in low-frequency zonal variations of the Southern Hemisphere circulation. *Tellus,* **42A,** 41–50.

Lee, S., and S. Feldstein, 1996: Two types of wave breaking in an aquaplanet GCM. *J. Atmos. Sci.,* **53,** 842–857.

Magnusdottir, G., and P. H. Haynes, 1996: Wave activity diagnostics applied to baroclinic wave life cycles. *J. Atmos. Sci.,* **53,** 2317–2353.

Nakamura, M., and R. A. Plumb, 1994: The effects of flow asymmetry on the direction of Rossby wave breaking. *J. Atmos. Sci.,* **51,** 2031–2045.

Ottino, J. M., 1989: *The Kinematics of Mixing: Stretching, Chaos, and Transport.* Cambridge University Press, 364 pp.

Simmons, A. J., and B. J. Hoskins, 1980: Barotropic influences on the growth and decay of nonlinear baroclinic waves. *J. Atmos. Sci.,* **37,** 1679–1684.

Thorncroft, C. D., and B. J. Hoskins, 1990: Frontal cyclogenesis. *J. Atmos. Sci.,* **47,** 2317–2336.

——, ——, and M. E. McIntyre, 1993: Two paradigms of baroclinic-wave life-cycle behaviour. *Quart. J. Roy. Meteor. Soc.,* **119,** 17–55.

Weiss, J., 1991: The dynamics of enstrophy transfer in two-dimensional hydrodynamics. *Physica D,* **48,** 273–294.

Yoden, S., and M. Yamada, 1993: A numerical experiment on two-dimensional decaying turbulence on a rotating sphere. *J. Atmos. Sci.,* **50,** 631–643.

——, M. Shiotani, and I. Hirota, 1987: Multiple planetary flow regimes in the Southern Hemisphere. *J. Meteor. Soc. Japan,* **65,** 571–586.

Yu, J.-Y., and D. L. Hartmann, 1993: Zonal flow vacillation and eddy forcing in a simple GCM of the atmosphere. *J. Atmos. Sci.,* **50,** 3244–3259.